




Event-based discrete PI controllers robustness analysis through sampled describing function technique

Oscar Miguel-Escrig and Julio-Ariel Romero-Pérez 

Department of System Engineering and Design, Universitat Jaume I, Castelló de la Plana, Spain

ABSTRACT

In this work, the robustness of discrete PI controllers when used with a Symmetric-Send-On-Delta (SSOD) sampling law is addressed. Hitherto, the continuous Describing Function has been employed as a suitable tool to evaluate the robustness of such systems to limit cycle oscillations induced by the SSOD. However, due to the discrete implementation of the controllers in most of the actual applications, the Sampled Describing Function technique is used in this work to provide a more realistic approach, which takes into account the effect of both the SSOD and sampling period of the discrete controller on inducing such oscillation. A simple measure has been developed to characterise the robustness of these systems and it has been tested through several examples, showing its validity in predicting the apparition or avoidance of limit cycles. This measure has been used to evaluate the robustness of some spread tuning rules applied to a wide batch of systems reflecting the dynamics of most processes in the industry.

ARTICLE HISTORY

Received 23 October 2020
Accepted 26 July 2021

KEYWORDS

Event-based-PI; SSOD; robustness; discrete control

1. Introduction

Event-Based Control (EBC) constitutes a solid alternative to classical time driven control on distributed control systems because it reduces the data drop out, decreasing the delays and minimising the packet losses in the communication networks. These controllers attain this objective as a consequence of their data send policy, which only sends new data when significant changes on the state of the system are produced, instead of periodically as classical time driven controllers do.

Therefore, this data send policy becomes crucial in EBC, because it is in charge of generating the events for the execution of the controller's algorithm. Among the different event generation techniques, the ones based on the signal quantification have become more important because of their ease of implementation. That is the case of the well-known Send-On-Delta (SOD) sampling strategy, which sends data whenever the signal changes more than a certain value δ from the last sample. This sampling technique has been used in several works proving its effectiveness in terms of control performance and communication reduction (Dormido et al., 2008; Ploennigs et al., 2010).

Several variations on the SOD sampling strategy have been presented, most of them considering the thresholds fixed and no longer depending on the last value taken. Among these variations, the Regular Quantisation was studied in terms of robustness in Romero Pérez and Sanchis Llopis (2017), and a variation of this last sampling strategy was presented in Miguel-Escrig and Romero-Pérez (2020), in which a customisable hysteresis was added to the sampling to avoid bursts of events due to noise. However, one of the most known variations of the SOD sampling was presented in Beschi et al. (2012), and it is known as Symmetric-Send-On-Delta (SSOD). This strategy presents

fixed thresholds of value δ and introduces a hysteresis of the same value δ , being its input-output relationship symmetric. Some guidelines for tuning SSOD based PI controllers have been provided in Beschi et al. (2014a) and Romero et al. (2014).

One of the main points in the analysis and design of event-based control systems is the existence and avoidance of limit cycle oscillations in the closed-loop response. The characterisation of steady-state oscillations for different types of systems under an SSOD sampling strategy has been presented in Chacón et al. (2013). This analysis has been treated in other works using the Describing Function (DF) technique (Romero & Sanchis, 2016), in which, in addition, tuning methods for PI controllers within a control structure with an SSOD sampler have been obtained. The use of the DF allows extending some concepts of the classical control theory, as the gain and phase margins, to the analysis and design of EBC systems. However, other analysis techniques can be used like the Tsytkin method, which has been specifically used to analyse the robustness of SSOD-PID structures in Miguel-Escrig et al. (2020).

In all the theoretical studies about SSOD-based control systems a continuous approach has been adopted towards the controller implementation, i.e. the PID is considered to be continuous and therefore all the results have been obtained under this assumption. In networked control systems, however, the controllers are always implemented in microprocessor-based devices considering a discrete approximation. The aim of this paper is to study the effect of the sampling time in the robustness to limit cycle oscillations when a discrete implementation of the PI controller is used jointly with the SSOD sampling strategy, as is the cases of the practical applications of the SSOD-PI presented in Beschi, Pawlowski et al. (2014), Beschi et al. (2014b), Romero et al. (2015), Rodríguez-Miranda et al. (2019), and

Rodríguez-Miranda et al. (2019). In neither of those papers, the influence of this parameter has been addressed.

Tuning methods for continuous PID are applied by the control practitioners in many industrial settings without bearing in mind that discrete versions of the controllers are executed in microprocessor-based systems. In most of these cases, the digital implementation of the controller does not have a detrimental effect in the loop because the sampling frequency used by the control algorithm is high enough to consider the controller as a continuous one. In this sense, it should be taken into account that the sampling time required for some common process variables such as flow, level, pressure or temperature is in the order of seconds meanwhile the commercial digital controllers have sampling intervals in the order of tens of milliseconds.

Despite the aforementioned fact, it is well known that the sampling time plays an important role in discrete time control systems. High values of sampling time could degrade the control performance or even produce instability. On the other hand, the minimum value of the sampling interval is limited by hardware and software restrictions of the microprocessor-based system where the control algorithms are executed. Because of the relevance of the sampling time, several criteria have been developed for selecting this parameter taking into account both the frequency or time response of the control loop (Isermann, 1989). A general rule of thumb for the PI controllers states the sample time in the range of 0.1–0.3 of integral time in order to obtain good performance and acceptable robustness of the control systems (Astrom & Wittenmark, 1997).

This paper addresses the robustness of SSOD-based control systems when a discrete PI is used. This consideration matches with the reality of computer-based implementation of controllers which are almost executed as a periodic algorithm. The analysis is based on the Sampled Describing Function (Kuo, 1963) which takes into account the SSOD quantification and the execution period of the controller. The main characteristics of this DF have been studied, revealing the influence of its parameters in the behaviour of this kind of control systems. Some guidelines are given to evaluate the existence of limit cycle using a new robustness measure proposed in the paper. Because of the lack of specific tuning rules for the scheme under study, the robustness of controllers provided by several classical and spread tuning rules for continuous PI has been evaluated, namely, Ziegler-Nichols (Ziegler & Nichols, 1942), AMIGO (Åström & Hägglund, 2004), One-Third (Hägglund, 2019) and SIMC (Skogestad, 2003) tuning rules. These methods have been applied to a batch of models that gather the most common dynamics in industrial processes, and their robustness in the studied loop structure has been evaluated using the proposed measure.

The paper is organised as follows. In Section 2, the loop structure and the general problematic are presented. In Section 3, the Sampled Describing Function that characterises the non-linear behaviour of the system is presented and studied. In Section 4, guidelines about how to perform the stability analysis are given, offering a systematic approach to evaluate the robustness and proposing a specific robustness measure. In Section 5, several tuning methods are used to tune controllers for a given batch of models and their robustness in the proposed loop structure is evaluated. Finally, in Section 6 the conclusion about the work is drawn.

2. Problem statement

Let us consider the networked control system presented in Figure 1, where $C(s)$ and $G(s)$ are the controller and the process transfer functions respectively, y_r is the reference signal to be tracked, y is the controlled output, and p is the disturbance input. The controller is assumed to be located near the actuator and the sensor sends samples of the process output represented by y (it could also be of the tracking error e) to the controller through the communication network whose communication delays are modelled by the term $\exp(-t_d s)$. The sensor unit employs an SSOD strategy for sampling the input signal: a new value $e^* = i\delta$, $i \in \mathbb{Z}$ is sent to the ZOH when e crosses the $i\delta$ levels and \bar{e} maintains its value for $\pm\delta$ variations around the $i\delta$ levels. This behaviour is described by Equation (1). It is worth remarking that other sampling strategies such as RQH presented in Miguel-Escrig and Romero-Pérez (2020) or asymmetric multi-level relays could be used, but SSOD is simpler to implement, has more literature associated addressing the tuning of controllers under this sampling and has been proved in several practical environments.

$$\bar{e}(t) = \begin{cases} (i+1)\delta & \text{if } (\bar{e}(t^-) = i\delta) \text{ \& } (e(t) \geq (i+1)\delta) \\ (i-1)\delta & \text{if } (\bar{e}(t^-) = i\delta) \text{ \& } (e(t) \leq (i-1)\delta) \\ i\delta & \text{if } e(t) \in [(i-1)\delta, (i+1)\delta] \end{cases} \quad (1)$$

This schema, and the control problem associated to it, was first proposed in Beschi et al. (2012) and it has been treated in different ways in the literature. In Beschi et al. (2014a), a tuning method for this kind of structure based on other tuning rules such as AMIGO (Hägglund & Åström, 2002) and SIMC (Skogestad, 2003) tuning rules was presented. In Romero et al. (2014) and Romero and Sanchis (2016), the authors rely on the DF approach to characterise the robustness against limit cycles produced by the SSOD non-linearity and propose a tuning method that takes this fact into account. In Miguel-Escrig et al. (2020), the Tsytkin method has been used to better characterise the

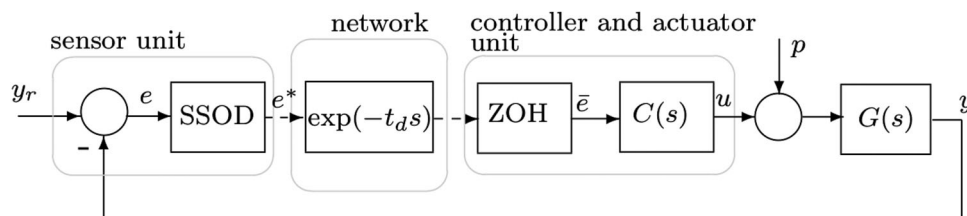


Figure 1. General approach to networked control systems with SSOD sampling strategy.

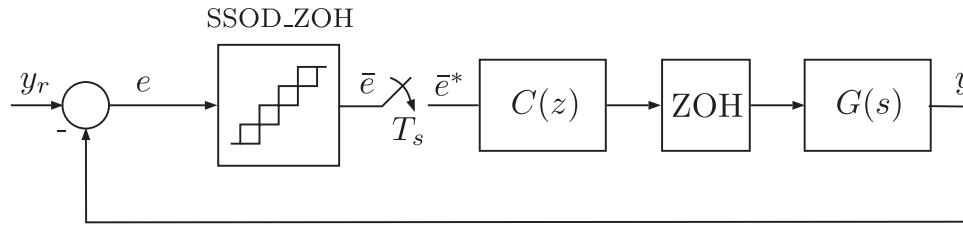


Figure 2. Sampled system configuration with SSOD non-linearity.

robustness to limit cycle of this kind of systems without the restrictions imposed by the DF about the filtering properties of $G(s)$.

The works mentioned above follow the approach of considering a continuous controller in the loop. However, this approach can induce to unexpected errors when the controllers are implemented in computer-like devices such as PLCs or other electronic cards. This fact modifies the approach to the problem presented in Figure 1, because neither the signal that arrives to the controller nor the controller is continuous; instead the signal is periodically sampled by the controller module to recalculate the control action, which is kept constant during the sampling time.

With the considerations already described above, the system in Figure 1 admits the Hammerstein–Wiener representation presented in Figure 2, being the block SSOD_ZOH the combination of the SSOD and ZOH blocks, and the implementation of the discrete PI being modelled by Equation (2), which has been obtained by applying the bilinear transform. This new block diagram describes the actual problem behind the networked control systems under study more accurately.

$$C(z) = K_p + \frac{K_p T_s z + 1}{T_i z - 1}. \quad (2)$$

One of the main issues when dealing with this kind of systems is the apparition of limit cycle oscillations, which are induced by the SSOD non-linear behaviour and sampling. In Figure 3, a typical limit cycle oscillation is shown. As it can be seen, the error signal e is not only quantified by the SSOD non-linearity, which results in \bar{e} , but it is also sampled afterwards, obtaining the samples \bar{e}^* , which constitute the input to the controller to compute and actualise the control action.

This quantification and posterior sampling constitute the source of limit cycle oscillations apparition. Therefore, to evaluate the robustness of a given system, an analysis methodology which takes into account the peculiarities of this kind of sampled system is presented.

3. Sampled describing function

To study non-linear systems with sampling elements, as that shown in Figure 2, there exist several methods, some of them exact as the one presented in McNamara and Atherton (1984), but very complicated for practical uses. Other methods like the ones based on the Describing Function offer an approximate estimation of the robustness, which is precise when a filtering linear part is present, while being easier to develop. Two variations on the original Describing Function technique can be

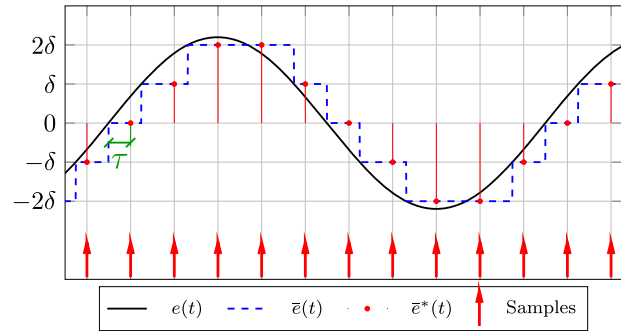


Figure 3. Sine wave in black, quantified by the SSOD_ZOH block in dashed blue, and sampled according to a given sampling period in red (sampling time indicated with red arrows).

used in this case, namely, the z -transform Describing Function (Kuo, 1960) and the Sampled Describing Function (Kuo, 1963), which will be used in this paper due to its simplicity (Gelb & Van der Velde, 1968).

The condition to avoid limit cycle oscillations is defined by

$$G_{ol}(j\omega) \neq -\frac{1}{\mathcal{N}}; \quad \forall \omega, \quad (3)$$

where $G_{ol}(j\omega)$ represents the open-loop transfer function of all the linear elements, i.e. network delay, controller, ZOH and system. \mathcal{N} is the Describing Function of the non-linear part, which in this case characterises the SSOD_ZOH block and the sampler. It can be proven (see Appendix A) that the Describing Function \mathcal{N} is given by the following equation:

$$\begin{aligned} \mathcal{N}(\delta/A, r, \tau, T_s) &= \frac{2\delta}{\pi T_s A} \sum_{k=-\infty}^{\infty} \frac{e^{-jk2\pi\tau/T_s}}{rk-1} \\ &\times \left[\sum_{i=1}^{m-1} \left\{ \left(-\sqrt{1 - \left(\frac{i\delta}{A}\right)^2} + j\frac{i\delta}{A} \right)^{rk-1} \right. \right. \\ &\quad \left. \left. - \left(\sqrt{1 - \left(\frac{i\delta}{A}\right)^2} + j\frac{i\delta}{A} \right)^{rk-1} \right\} \right. \\ &\quad \left. - \left(\sqrt{1 - \left(\frac{m\delta}{A}\right)^2} + j\frac{m\delta}{A} \right)^{rk-1} + (-1)^{rk-1} \right], \quad (4) \end{aligned}$$

where $m = \lfloor \frac{A}{\delta} \rfloor$ is the number of levels crossed, τ is the lag between the zero-crossing of the signal and the first sample

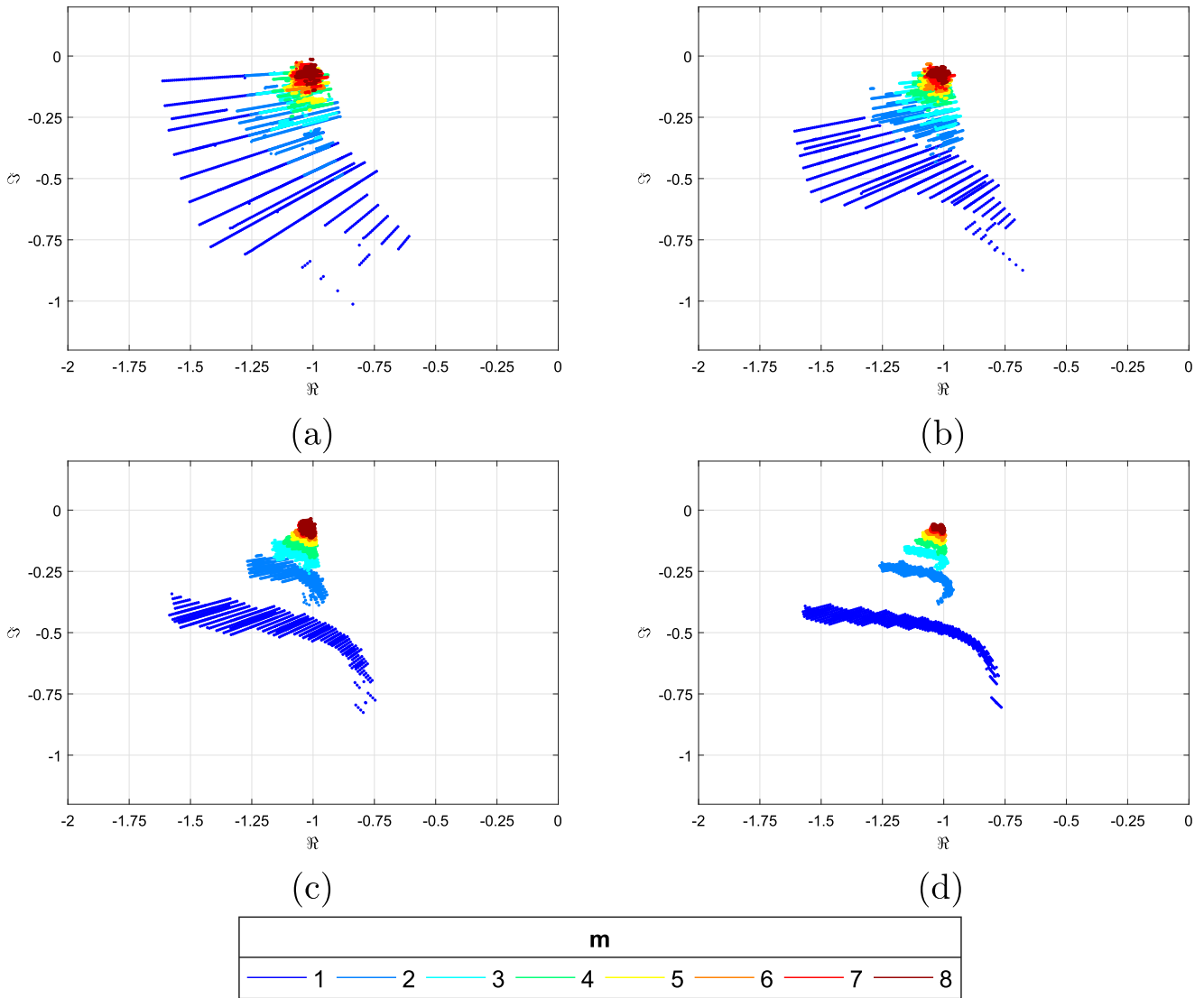


Figure 4. Sampled DF for different values of r , all of them considering $T_s = 1$: (a) $r = 10$, (b) $r = 20$, (c) $r = 50$, (d) $r = 100$.

taken (see Figure 3) and r is the ratio between the oscillation period T_o and the sampling period T_s .

From expression (4) it can be observed that, as in the case of the continuous DF of the SSOD quantisation (Romero & Sanchis, 2016), the shape of the sampled DF does not depend on the specific value of δ , but on its relationship with the amplitude A of the induced oscillation, which is expressed by the quotient δ/A . Therefore, the robustness does not depend on the quantisation level since varying δ will also modify the amplitude of the oscillation proportionally, resulting in the same ratio A/δ and, consequently, in the same points on the Nyquist diagram.

According to Gelb and Van der Velde (1968), r must be an integer value, otherwise the oscillation may contain harmonic components with frequencies lower than the fundamental frequency, which cannot be discarded with the filtering hypothesis. In addition, in those cases where r is considered to be odd, the samples taken in each semi-period of the oscillation are different, this leads to an asymmetry which can be relevant for those cases where a low number of samples per period are taken; in the other cases this difference is irrelevant.

Figure 4 depicts the shapes of $-1/\mathcal{N}$ for different values of r . The locus of $-1/\mathcal{N}$ is composed of several branches, one for each value of m , and each of them has been represented with a different colour. Bigger values of m tend to approximate the traces of the DF to the point $(-T_s, 0)$ and as the value of m is reduced the branches expand towards the third quadrant. The clearer case is the one presented in Figure 4(d) where each branch is visibly well defined and it reassembles the DF of the SSOD (without sampling) (Romero & Sanchis, 2016). This happens because for that Sampled DF the ratio r is big enough to consider the effect of the sampling negligible. Nevertheless, for the other cases it can be seen how decreasing that ratio tends to widen the size of the branches, deforming them and making them unintelligible from one another.

In Gelb and Van der Velde (1968), the concept of oscillation mode is presented for a relay non-linearity. In that case, a n, n mode is defined as a cycle in which n positive drive pulses are followed by n negative drive pulses. This concept can be applicable to the oscillations produced by the non-linear structure

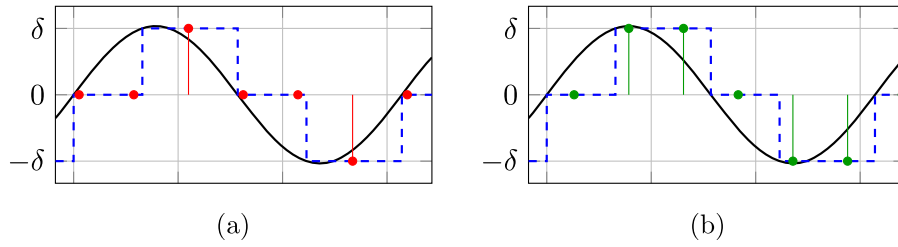


Figure 5. Sine wave quantified by an SSOD and sampled resulting in two different oscillation modes: (a) $\bar{e}^*(kT_s) = 0, 0, \delta$ and (b) $\bar{e}^*(kT_s) = 0, \delta, \delta$.

studied in this paper introducing a slight difference due to the non-linearity characteristics.

Consider a one-levelled oscillation ($m = 1$), sampled in such a way that $r = T_o/T_s = 6$. With this sampling rate, six samples are taken in an oscillation period. In a semi-period, the values that these samples can have are either $\bar{e}^*(kT_s) = 0, 0, \delta$ or $\bar{e}^*(kT_s) = 0, \delta, \delta$ for $k = 1, 2, 3$. Both examples are shown in Figure 5 (a and b) respectively. Note that on the other semi-period, the samples for $k = 4, 5, 6$ would be the same but with opposite sign. These two combinations are the only two possible modes for the considered sampling rate maintaining the amplitude of the oscillation.

Focusing on the simpler mode type, which are those where $m = 1$, the number of modes for a given value of r can be characterised as follows. As it has been shown, the modes in SSOD sampled oscillations are characterised by samples in a lower level $\bar{e}^* = 0$ and samples in a high level $\bar{e}^* = \delta$ and its symmetric in the second semiperiod. In addition, as the amplitude of the oscillation increases the temporal frame before \bar{e} commutates to a high level is reduced. Therefore, the number of modes can be obtained as the difference between the maximum and minimum number of samples that fit in the temporal frame before commutation. Then, considering the two extreme cases for the amplitude in the case $m = 1$, which are $A = \delta$ and $A = 2\delta$, and as e is a sinusoid, the time in which the switch is produced ($e = \delta$) can be obtained, which is $t_1 = T_o/4$ and $t_2 = T_o/12$. The number of samples that fit in that temporal frame is obtained dividing by T_s , and then, just counting the difference between the maximum and minimum number of samples that fit in that temporal frame, the number of modes for a given r in $m = 1$ is obtained as

$$n^\circ \text{ modes} = \left\lceil \frac{r}{4} \right\rceil - \left\lfloor \frac{r}{12} \right\rfloor + 1. \quad (5)$$

From this expression, it can be observed that the number of possible modes increases with the sampling ratio r , intuitively, decreasing the sampling period increases the number of samples in that temporal frame, being the difference between the extreme cases greater.

The influence of the ratio r on the oscillation modes is reflected in the DF traces. In Figure 6, it has been represented the branch that corresponds to $m = 1$ of the Sampled DF with $r = 50$. It can be seen some overlapping rhomboid regions (one of them surrounded in red), which are crossed by several straight lines. Each of those rhomboid regions corresponds to a different oscillatory mode, i.e. the oscillations obtained when intersecting those regions have a certain number of samples in each level.

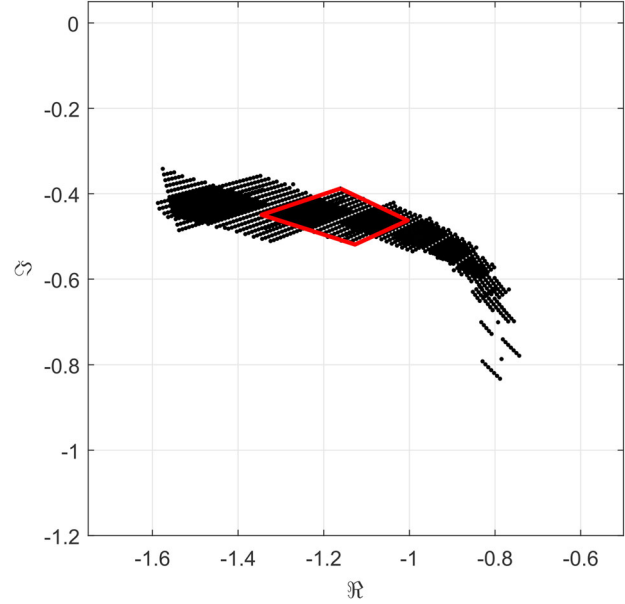


Figure 6. Detail of the branch $m = 1$ of the Sampled DF with $T_s = 1$ and $r = 50$ with a mode region highlighted.

Within the rhomboid regions, some straight lines appear. Each of these series of traces corresponds to a different initial lag τ when evaluating the DF swapping the ratio δ/A . This implies that multiple combinations of ratios δ/A and initial lags τ can generate the same limit cycle oscillation. This can be easily seen from the oscillation mode shown in Figure 5, where the represented modes can be obtained for different combinations of the sine amplitude A and initial sampling delay τ .

The oscillation modes depend on the sampling rate, but also on the ratio δ/A , which propitiates the existence of modes in which several levels are crossed ($m > 1$). This kind of modes involves an additional complexity for its analysis due to the apparition of a curious phenomena: if the sampling rate is not sufficient, a level may not have any sample on it, resulting in more overlapping regions. As the main goal of this contribution is to avoid any type of oscillation modes, we will not focus on their study, however, it is important to notice that the dispersion of the DF traces with r can be explained with the understanding of the concept of modes. With low ratios of r fewer number of modes are possible and more combinations of parameters are possible to obtain them, generating a great dispersion of the DF traces. On the other hand, with higher ratios of r more modes (rhomboid regions) appear, but they are smaller because the parameters admit less variation to maintain the mode.

4. Stability analysis

One of the main considerations when studying the networked control systems presented in this paper is the avoidance of limit cycle oscillations induced by SSOD sampling law. These oscillations can be prevented if the condition described by Equation (3) is fulfilled, which relates the non-linear part, characterised by the DF \mathcal{N} , and the linear part of the system.

Considering first the linear part of the system in Figure 2, the open-loop transfer function $G_{ol}(s)$ that includes the discrete controller $C(z)$, the ZOH, the time delay introduced by the network and the system $G(s)$ must be obtained. The transfer function of the ZOH is

$$\text{ZOH}(s) = \frac{1 - e^{-sT_s}}{s}.$$

Then, the transformation $z = e^{sT_s}$ is applied to the transfer function of the discrete controller, given by Equation (2), to obtain the starred transform of the controller $C^*(s)$, obtaining

$$G_{ol}(s) = C^*(s)\text{ZOH}(s)G(s). \quad (6)$$

To facilitate the stability analysis, condition (3) has been rewritten as

$$\frac{G_{ol}(s)}{T_s} \neq \frac{-1}{\mathcal{N}'}; \quad \forall \omega, \quad (7)$$

where

$$\begin{aligned} \mathcal{N}'(\delta/A, r, \theta_s) &= \frac{2\delta}{\pi A} \sum_{k=-\infty}^{\infty} \frac{e^{-jk\theta_s}}{rk-1} \\ &\times \left[\sum_{i=1}^{m-1} \left\{ \left(-\sqrt{1 - \left(\frac{i\delta}{A}\right)^2} + j\frac{i\delta}{A} \right)^{rk-1} \right. \right. \\ &\quad \left. \left. - \left(\sqrt{1 - \left(\frac{i\delta}{A}\right)^2} + j\frac{i\delta}{A} \right)^{rk-1} \right\} \right. \\ &\quad \left. - \left(\sqrt{1 - \left(\frac{m\delta}{A}\right)^2} + j\frac{m\delta}{A} \right)^{rk-1} + (-1)^{rk-1} \right], \quad (8) \end{aligned}$$

which essentially is the same expression that (4) without T_s in the denominator because it has been moved to the left term of Equation (7). Additionally, the expression $2\pi\tau/T_s$ in the exponential of \mathcal{N} has been substituted by θ_s . As $\tau \in [0, T_s[$, then $\theta_s \in [0, 2\pi[$. These small changes make \mathcal{N}' dimensionless and prevent it from being scaled by T_s . Therefore, similar to the continuous DF for SSOD, \mathcal{N}' tends to $(-1, 0)$ as m increases, regardless of the sampling period. Additionally, to homogenise the notation in the stability condition (7), let us express the frequency ω in terms of r and the sampling frequency ω_s :

$$\frac{G_{ol}\left(j\frac{\omega_s}{r}\right)}{T_s} \neq \frac{-1}{\mathcal{N}'(\delta/A, r, \theta_s)}; \quad \forall r \in \mathbb{Z}, \quad r_{\min} < r < r_{\max} \quad (9)$$

Even though the frequency ω does not appear explicitly in Equation (9), it is hidden within the ratio $r = T_o/T_s = \omega_s/\omega_o$

because each evaluated frequency ω is a candidate to become the oscillation frequency ω_o . Therefore, as both sides of the Equation (9) depend on the evaluated frequency it is important to know the range of ω where this condition must be evaluated to check the existence of limit cycles. In this sense, it is worth noting that the traces of the negative inverse of the presented DF lie in the third quadrant of the polar plot, see Figure 4, thus the frequencies to be evaluated must be those for which $G_{ol}(j\omega)$ lies in this quadrant too. Even if the range of frequencies placed in the third quadrant is very wide, it is not necessary to check all of them. In the lines below, the guidelines about the calculation of this range and the stability analysis are given.

As it has been commented before, the DF traces lie in the third quadrant. Thus, considering a given sampling frequency ω_s , the frequencies in this quadrant that make r an integer should be evaluated. The minimum value of r will provide the highest frequency placed within the third quadrant. It is known that the crossover phase frequency ω_{cp} corresponds to a point of G_{ol} over the real axis between the second and third quadrants, therefore, using this frequency, the minimum value of r can be easily determined by

$$r_{\min} = \left\lceil \frac{\omega_s}{\omega_{cp}} \right\rceil. \quad (10)$$

The maximum value of r can be also established by analysing the shape of the DF traces under study. It is worth noting that, for a given sampling frequency, higher values of r correspond to lower frequencies ω . The increment of r also results in traces of \mathcal{N}' more and more similar to the continuous DF traces for the SSOD, which lie in a well-defined zone in the third quadrant. To study the possible intersection between $-1/\mathcal{N}'$ and G_{ol}/T_s , there is no need to evaluate points beyond the extension of these traces, whose further point from the origin in the Nyquist diagram is at a distance of 1.62 units. Then, the point of $G_{ol}(s)/T_s$ with modulus equal to 1.62 determines the lowest frequency that must be evaluated to check intersection.

The previous ideas are illustrated in Figure 7. The negative inverse of the Sampled DF with a high value of r is represented in red, which is very similar to the continuous DF of the SSOD, represented in black. This shows that the Sampled DF asymptotically tends to the continuous DF as r increases, and consequently the range of r to study intersection can be bounded as commented before. It can also be seen how the further point of $-1/\mathcal{N}'$ defines the point of G_{ol} with lowest frequency that could intercept the negative inverse of DF: $|G_{ol}(s)/T_s| = 1.62$. This point determines the maximum value of r . The range of frequencies that need to be evaluated to check intersection has been highlighted in green.

Analytically, the maximum value for r can be easily obtained with

$$r_{\max} = \left\lceil \frac{\omega_s}{\omega'_{cg}} \right\rceil, \quad (11)$$

where ω'_{cg} is the frequency where the open-loop transfer function has the maximum modulus of the DF trace:

$$\left\| \frac{G_{ol}(j\omega'_{cg})}{T_s} \right\| = 1.62. \quad (12)$$

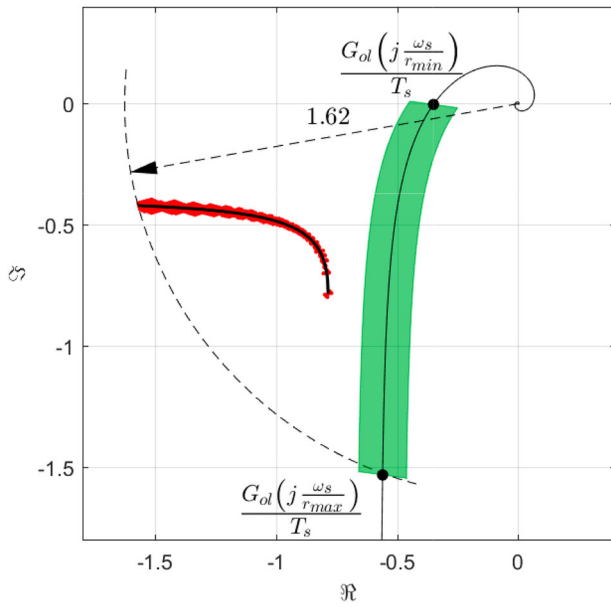


Figure 7. Graphical representation of the evaluated range of frequencies.

To clarify the use of the stability condition (9) and the estimation of the minimum and maximum values of r let us introduce the following example.

Example 4.1: Consider a process with transfer function:

$$G(s) = \frac{1}{(s+1)^3}.$$

A PI controller is tuned according to Romero and Sanchez (2016), where a tuning method is presented to prevent limit cycle oscillations in the control scheme in Figure 1. To achieve that, the method avoids the intersection between the open-loop transfer function and the negative inverse of the continuous DF of the SSOD sampler by assuring a minimum phase margin between $G_{ol}(j\omega)$ and the critical point of $-1/\mathcal{N}'$, which is set to $\Phi_{m,SSOD} = 10^\circ$, while fulfilling a minimum gain margin restriction, which is fixed to $\gamma_{cp} \geq 6$ dB. The obtained parameters for the controller are $K_p = 1.35$ and $T_i = 2.38$ and the representation of the open-loop transfer function with the traces of the inverse negative of the continuous DF in the Nyquist diagram that validates this controller in the continuous case is presented in Figure 8.

It is worth remarking that the continuous PI with the previous parameters assures the avoidance of limit cycle oscillations in the control scheme in Figure 1. Our goal, however, is to analyse the existence of limit cycles when using these parameters in a discrete PI controller $C(z)$ in the control scheme in Figure 2. Let us consider the trapezoidal form of the PI with a sampling period $T_s = 0.5$ s.

The minimum value of r has been obtained according to Equation (10) for which the crossover phase frequency of $G_{ol}(s)/T_s$ was calculated ($\omega_{cp} = 1.11$ rad/s) and the minimum value of r results in $r_{\min} = \lceil \omega_s/\omega_{cp} \rceil = \lceil 12.57/1.11 \rceil = 12$. Analogously, the crossover gain frequency of $G_{ol}(s)/1.62/T_s$ has been obtained ($\omega'_{cg} = 0.38$ rad/s) and Equation (11) has been

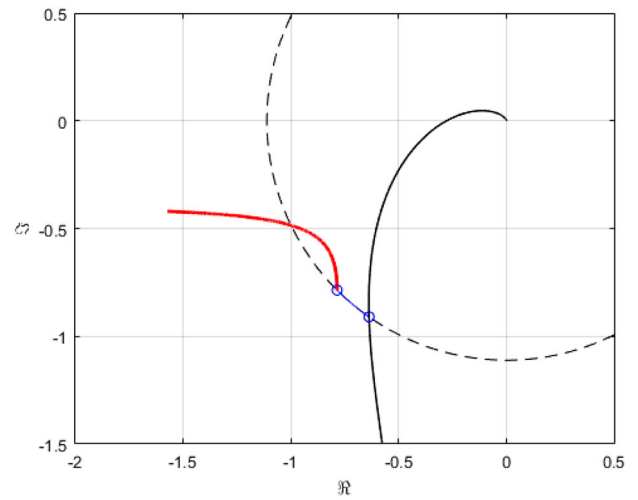


Figure 8. $G_{ol}(j\omega)$ and $-1/\mathcal{N}'$ for the continuous case. The presented PI avoids limit cycle oscillations in this case.

used to calculate the maximum bound of r , which results in $r_{\max} = \lceil \omega_s/\omega'_{cp} \rceil = \lceil 12.57/0.38 \rceil = 33$.

Figure 9(a) shows the Nyquist diagram of $G_{ol}(s)/T_s$ and the traces of the negative inverse of the Sampled DF for the level $m = 1$. The points corresponding to several values of r between the bounds obtained above and their respective normalised Sampled DF traces, given by $-1/\mathcal{N}'(r)$, have been highlighted each in a different colour. Then, according to condition (9), a limit cycle takes place if some point and trace highlighted with the same colour intersect. Due to the complex shape of the traces, which overlap one to another, the previous condition is difficult to be evaluated from Figure 9(a). A more clear representation is obtained by substituting the traces by their convex hull as in Figure 9(b). Now the verification of the stability condition is easier: if $G_{ol}(j\omega_s/r)/T_s$ lies within the convex hull that contains $-1/\mathcal{N}'(r)$, the system could present limit cycle oscillations. In this case, $G_{ol}(j\omega_s/20)$ is placed within the convex hull of $-1/\mathcal{N}'(20)$, therefore, a limit cycle oscillation could exist for $r = 20$. The system has been tested in simulation with an SSOD sampler with $\delta = 0.1$. The results from the simulation are presented in Figure 10, where the controlled output and the control action temporal responses to a unitary step change in the reference and disturbance inputs are depicted considering both the discrete and continuous controllers. As can be seen, no oscillations are observed in the response of the continuous controller since the limit cycles are avoided by the tuning method. On the other hand, the response with the discrete controller presents limit cycle oscillations, whose frequency has been measured to be $\omega_s/20$, which corresponds to the point of the open-loop transfer function placed within its convex hull in Figure 9(b). This example shows how the discrete version of a stable continuous controller could induce limit cycle oscillations in the control loop. This fact stress the importance of the analysis presented in this paper.

4.1 Robustness measure

In Example 4.1, it can be noted that only branches with $m = 1$ have been considered. As can be seen in Figure 4, no matter the

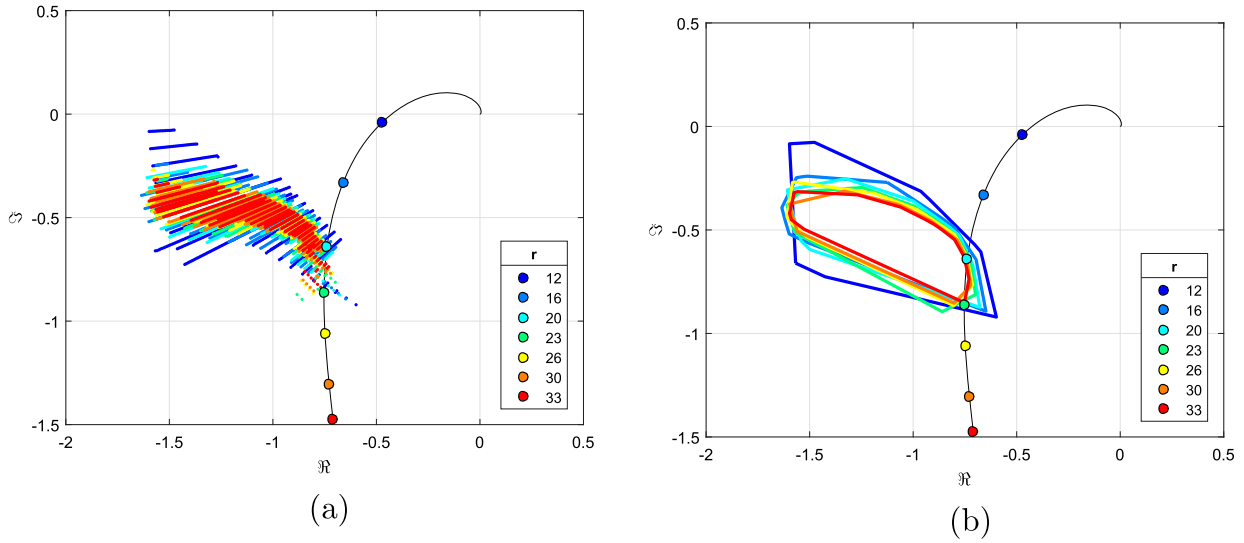


Figure 9. Sampled DF for $m = 1$ with $T_s = 0.5$ considering different values of r : (a) original $-1/\mathcal{N}'$ representation and (b) $-1/\mathcal{N}'$ replaced by its respective convex hull.

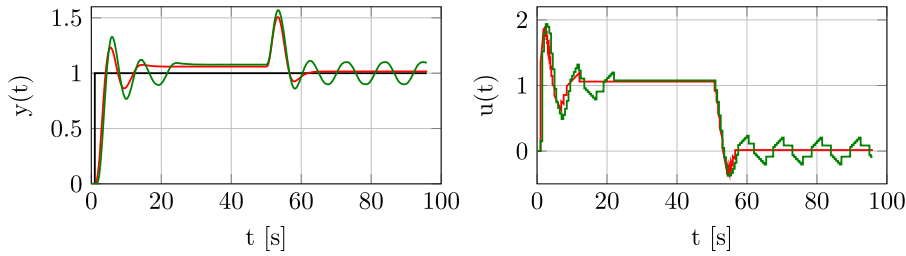


Figure 10. Controlled output and control action temporal response to a unitary step change in the reference and disturbance inputs with the discrete (green) and continuous (red) controller. The limit cycle predicted from the Sampled DF analysis can be observed.

value of r , the branches of $-1/\mathcal{N}'(r)$ shrink and move near to the real axis as m increases. Taking this into account, the shape of $G_{ol}(s)/T_s$ obtained with a PI controller for most of the process models is such that the distance between $G_{ol}(s)/T_s$ and $-1/\mathcal{N}'$ increases with m . Therefore, the nonintersection with the branches of $m = 1$ guarantees no intersections for $m > 1$. This fact was pointed out in Romero and Sanchis (2016) for the case of continuous PI and it would be demonstrated experimentally in the next section that this affirmation also holds for the sampled case. Consequently, only the branches of $m = 1$ need to be considered to define a robust margin to avoid limit cycles.

Under the previous assumption, and considering the stability condition given by Equation (9), a very simple robustness measure can be defined as the minimum distance between a point of Nyquist diagram and its respective convex hull containing the traces for a given value of r . We will refer to this measure as D_{ch} , and it can be formally defined as

$$D_{ch} = \min_{r_{\min} \leq r \leq r_{\max}} \left(\text{dist} \left(G_{ol}(j\omega_s/r)/T_s, CH(-1/\mathcal{N}'(r)) \right) \right) \quad (13)$$

where $\text{dist}(\cdot)$ denotes the Euclidean distance and $CH(\cdot)$ refers to the convex hull.

The following example illustrates the use of the proposed margin to measure the robustness to limit cycle oscillation.

Example 4.2: Consider a process whose transfer function is defined by

$$G(s) = \frac{1}{(s+1)^5}.$$

A PI controller has been tuned using AMIGO tuning rule (Åström & Häggglund, 2004) obtaining $K_p = 0.2564$ and $T_i = 2.891$. This method has been chosen because it has been proven that provides good robustness capabilities against limit cycle oscillations induced by the SSOD quantification (Miguel-Escrig et al., 2020). A sampling period $T_s = 1.9$ has been selected for the discrete implementation of the controller, which corresponds to a tenth of the rise time of the continuous response.

Once the discrete controller has been implemented in its trapezoidal form, the robustness analysis as described previously has been performed. The convex hulls and the evaluated frequency points for different values of r have been represented in Figure 11(a). Circles representing the minimum distances from each frequency point to its respective convex hull are also shown in the figure. From those distances the minimum, which we have named D_{ch} , is the one that corresponds to $r = 31$. As distinguishing it from all the convex hulls and circles from Figure 11(a) is not quite clear, it has been highlighted in Figure 11(b). In this case, the convex hull and the frequency in which D_{ch} is obtained have been highlighted while the other distances, which are greater than D_{ch} , have been represented in gray.

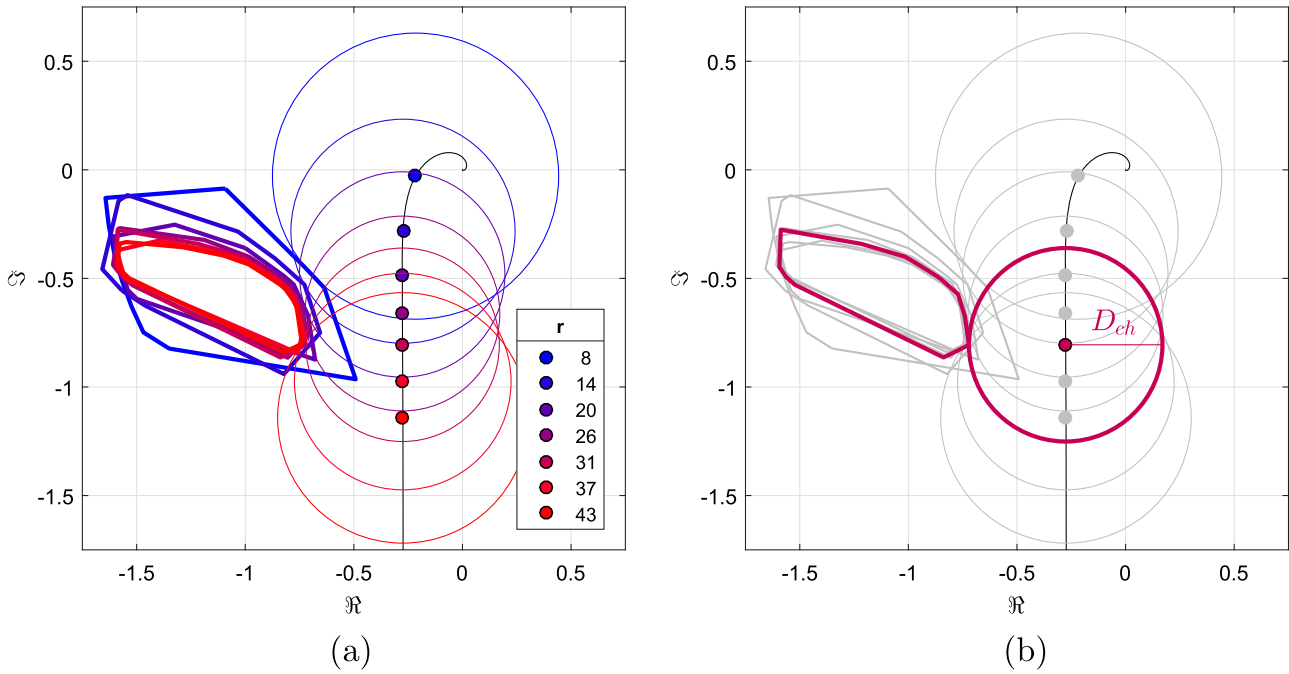


Figure 11. Representation of the distances from the evaluated points to their respective convex hull and detail of D_{ch} for the studied system: (a) all the distances to convex hull and (b) D_{ch} highlighted.

Therefore, as for this example we have obtained $D_{ch} = 0.45$ the system avoids limit cycle oscillations. To prove that, the system has been tested in simulation with a step change in the reference and disturbance inputs. The SSOD sampler used has a quantisation level $\delta = 0.1$. In Figure 12, the controlled output and control action temporal responses to a unitary step change in the reference and disturbance have been presented considering a continuous controller (in red) and a discrete controller (in green). As it can be seen, the system presents a smooth response and does not present limit cycle oscillations, as predicted by the robustness analysis, while not degrading significantly the performance provided by the continuous controller.

5. Robustness of continuous tuning rules

To illustrate the usefulness of the presented margin, it has been applied to study the robustness against limit cycle oscillations induced by the quantification and sampling of the SSOD. The discrete controller is implemented in its trapezoidal form as shown in Figure 2. The tuning methods for this study are Ziegler–Nichols (Ziegler & Nichols, 1942), AMIGO (Åström & Hägglund, 2004), One-Third rule (Hägglund, 2019) and SIMC (Skogestad, 2003). PI controllers have been tuned for the batch of models presented in (14), which describe a wide range of behaviours that can be found in real systems. The dynamic responses of the models in the batch have been approximated by First-Order Plus Time Delay (FOPTD) models to obtain the parameters of their respective controller.

$$G(s) = \frac{e^{-s}}{(Ts + 1)^2},$$

$$T = 0.01, 0.02, 0.05, 0.1, 0.2, 0.3, 0.5, 0.7, 1,$$

$$1.3, 1.5, 2, 4, 6, 8, 10, 20, 50, 100, 200, 500$$

$$G(s) = \frac{1}{(s + 1)(Ts + 1)^2},$$

$$T = 0.05, 0.1, 0.2, 0.5, 2, 5, 10$$

$$G(s) = \frac{1}{(s + 1)^n},$$

$$n = 3, 4, 5, 6, 7, 8$$

$$G(s) = \frac{1}{(s + 1)(\alpha s + 1)(\alpha^2 s + 1)(\alpha^3 s + 1)}, \quad (14)$$

$$\alpha = 0.1, 0.2, 0.3, 0.4, 0.5, 0.6, 0.7, 0.8, 0.9$$

$$G(s) = \frac{Te^{-L_1 s}}{(T_1 s + 1)(Ts + 1)},$$

$$T_1 + L_1 = 1, \quad T = 1, 2, 5, 10$$

$$L_1 = 0.01, 0.02, 0.05, 0.1, 0.3, 0.5, 0.7, 0.9, 1$$

$$G(s) = \frac{1 - \alpha s}{(s + 1)^3},$$

$$\alpha = 0.1, 0.2, 0.3, 0.4, 0.5, 0.6, 0.7, 0.8, 0.9, 1, 1.1$$

$$G(s) = \frac{1}{(s + 1)((sT)^2 + 1.4sT + 1)},$$

$$T = 0.1, 0.2, 0.3, 0.4, 0.5, 0.6, 0.7, 0.8, 0.9, 1$$

To obtain the sampling period for each controller a simple procedure has been followed. The closed-loop response of each system with its controller in continuous has been obtained and its rise time T_r has been measured. Then, the sampling period T_s has been obtained as $T_s = T_r/10$. With all the parameters obtained for the implementation of the discrete controller the robustness analysis as shown in the previous section has been done, obtaining the minimum distance to the convex hull D_{ch}

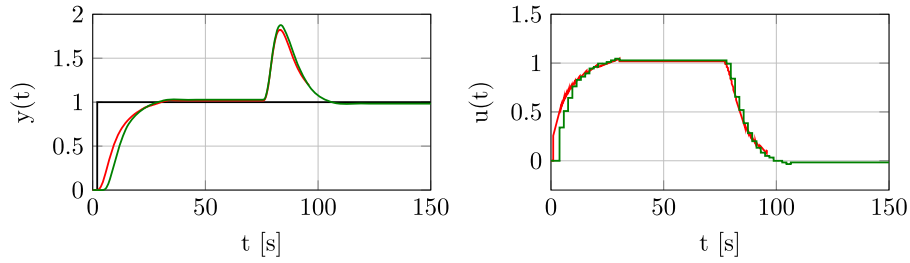


Figure 12. Controlled output and control action temporal response to a unitary step change in the reference and disturbance inputs with the discrete (green) and continuous (red) controller. The absence of limit cycle oscillations predicted by the Sampled DF analysis can be observed.

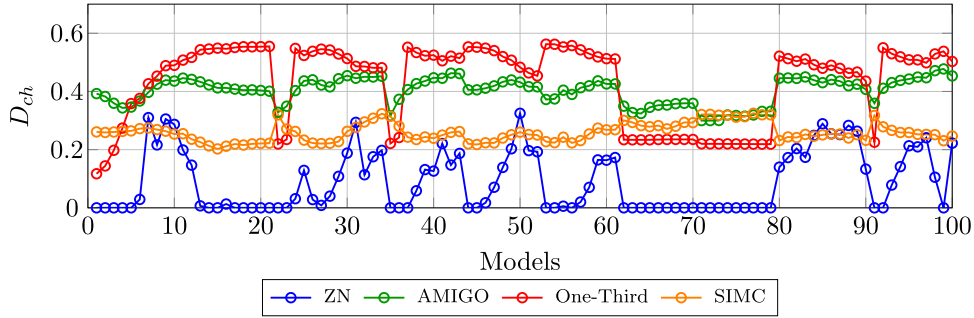


Figure 13. D_{ch} for the batch of processes with different controllers considering $T_s = T_r/10$.

for each system and controller in the batch. The results are presented in Figure 13.

The first result that can be observed in this figure is that Ziegler–Nichols controllers struggle to avoid limit cycle oscillations. On the other hand, the other tuning methods offer different degrees of robustness but in general they manage to avoid limit cycle oscillations.

Regarding the methods that consistently avoid these oscillations, it can be seen that AMIGO and SIMC offer a uniform level of robustness while One-Third rule presents several bumps. These bumps are caused because the closest convex hull, with respect to which the D_{ch} is measured changes. For example, for process 60 the closest convex hull is the one that encloses $-1/\mathcal{N}'(21)$, but for the process 62 the closest convex hull is $-1/\mathcal{N}'(3)$. The case of the process 62 is illustrated in Figure 14, where it can be seen how the convex hull of $-1/\mathcal{N}'(3)$ is larger than the rest, overtaking all of them and, therefore, defining D_{ch} . However, this situation is not desirable in practice since having only three samples per period could be insufficient for control purposes. Nevertheless, despite the presence of these extreme cases, One-Third rule consistently avoids limit cycle oscillations and it provides some of the highest robustness measures.

A second robustness analysis has been performed with a more conservative approach considering $T_s = T_r/20$. The obtained results are presented in Figure 15. As in the precedent case study, controllers tuned with Ziegler–Nichols method offer the lowest robustness in general lines, conducting most controllers to limit cycle oscillations. The other methods under study offer similar characteristics than with the previous sampling frequency. AMIGO and SIMC offer a more uniform level of robustness than the One-Third rule, which still presents some bumps in the measure D_{ch} even if the total amount has diminished.

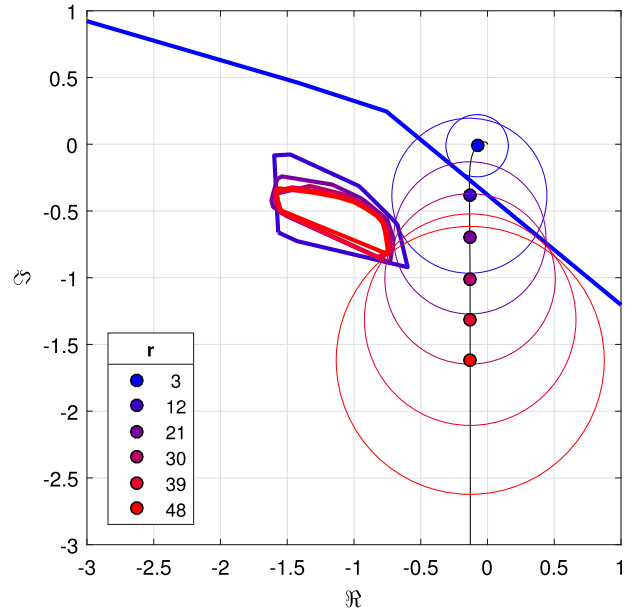


Figure 14. Some convex hull plots for process 62. The convex hull of $-1/\mathcal{N}'(3)$ overtakes the rest, defining D_{ch} .

In Figure 16, the difference in the robustness measure D_{ch} produced by the increase of the sampling frequency is presented. In this figure, it can be seen a behaviour that matches with the general principles of the discrete control, the robustness increases with the sampling frequency. In all the studied processes and methods in the batch, the robustness increases with the sampling frequency, being this rise greater for the One-Third rule. This tuning rule also presents a boost in the robustness for some processes, which are produced by avoiding some of the bumps in the robustness presented in Figure 13.

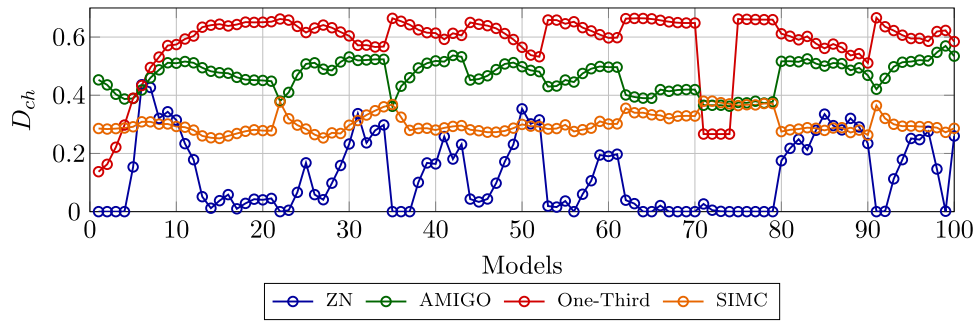


Figure 15. D_{ch} for the batch of processes with different controllers considering $T_s = T_r/20$.

As a consequence of increasing the sampling frequency, the value r_{min} has risen, avoiding large convex hull of undesirable situations, as the presented in Figure 14. The Ziegler–Nichols tuning rule also presents some bumps produced by a situation similar to the previously described.

This evaluation of some of the most used tuning rules designed for continuous processes reveals that Ziegler–Nichols tuning rule with the sampling criteria followed is not recommendable. In addition, it can be noted that the rest of tuning rules provide some degree of robustness against limit cycle oscillations and some interesting casuistic as the robustness bumps.

Remark 5.1: In general, a universally valid value of D_{ch} that assures good behaviour of the closed loop response is not known. However, values of D_{ch} in the order of 0.2–0.6 have been obtained from the previous study for the batch of processes with different tuning methods. Because some considered methods for tuning the PI provide acceptable temporal responses, even in a quasi-optimal sense as in the case of AMIGO method, then values of D_{ch} in this range could be considered reasonable to obtain good close loop performances.

5.1 Effect of sampling period on the performance

In general, discrete controllers have inferior performance over continuous control systems. This is sometimes explained due to the fact that sampled signals have less information than continuous signals. In order to study the effect of the sampling time on the performance of the discrete event-based control loop under study, the index IAE^* has been used, which is defined as

$$IAE^* = \frac{\overline{IAE}}{IAE_c},$$

where \overline{IAE} and IAE_c are the IAE indexes of the system response to a step-like disturbance with the discrete event-based controller and the continuous controller respectively. The study has been conducted for the controllers obtained in the previous section considering three different sampling rates: $T_s = T_r/20$, $T_s = T_r/10$ and $T_s = T_r/3$. The results are presented in Figure 17.

It can be seen that it does not exist a great difference in performance between the sampling periods $T_s = T_r/10$ and $T_s = T_r/20$, despite the fact that in those cases a significant difference in robustness was observed in Figure 16. In addition,

for a sampling period $T_s = T_r/3$ the performance decreases in almost every case with regard to the other sampling rates. This downgrade of the sampling frequency not only worsens the performance of the system, but it has also been observed a significant loss of robustness. In fact, in Figure 17 most of the values of IAE^* for this sampling rate have been omitted since their respective D_{ch} values were 0.

The robustness measure for the sampling rate $T_s = T_r/3$ is presented in Figure 18, where it can be seen that most of the controllers operating under this sampling rate will present an oscillatory behaviour since $D_{ch} = 0$. For those controllers that avoid limit cycle oscillations, it can be observed a significant loss of robustness comparing the values of D_{ch} presented in this figure with the values obtained for $T_s = T_r/10$ and $T_s = T_r/20$, which were presented in Figures 13 and 15 respectively. In summary, it can be concluded that the sampling rate has a strong influence in both the robustness and the performance which are improved as the sampling rate rise.

5.2 Influence of model uncertainties on D_{ch}

Regarding the uncertainties in parameters of the plants, it is clear the higher the value of D_{ch} the more admissible modelling error or variations in the parameters before limit cycle oscillation take place. In general, the uncertainties in the model can effect both the module and the phase of the G_{ol} . The uncertainties affecting the modules of G_{ol} , e.g. those in the process gain, only produce a radial displacement in $G_{ol}(s)/T_s$ which expands or shrinks as the gain increases or decreases respectively. Therefore, as convex hulls obtained for the calculation of D_{ch} remain invariant in this case, an increment in the process gain implies a reduction on D_{ch} because the critical points are getting closer to its respective convex hull.

The uncertainties that affect the phase of the process will modify the crossover phase frequency, modifying the value of r_{min} . In addition, this will produce a turn of $G_{ol}(s)/T_s$ in the Nyquist diagram, approaching or separating the critical points from their respective convex hull. Phase increment could take place if the time delay rises, which would add ωL radians to the phase of $G_{ol}(s)/T_s$, where L is the delay. In that case, the robustness measure D_{ch} would decrease since the values of r to evaluate would be lower, increasing the dispersion of the Sampled DF traces, and the turn on $G_{ol}(s)/T_s$ would approach the critical points to those convex hulls. Other variations on the open-loop transfer function could be induced by fluctuations on model

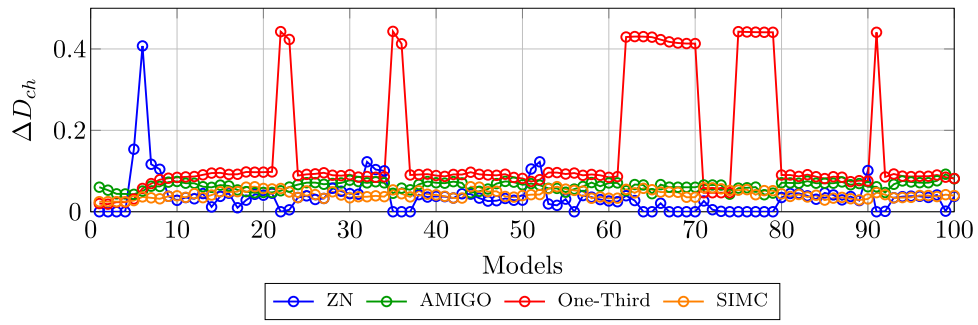


Figure 16. Variation of D_{ch} produced by an increase in the sampling frequency.

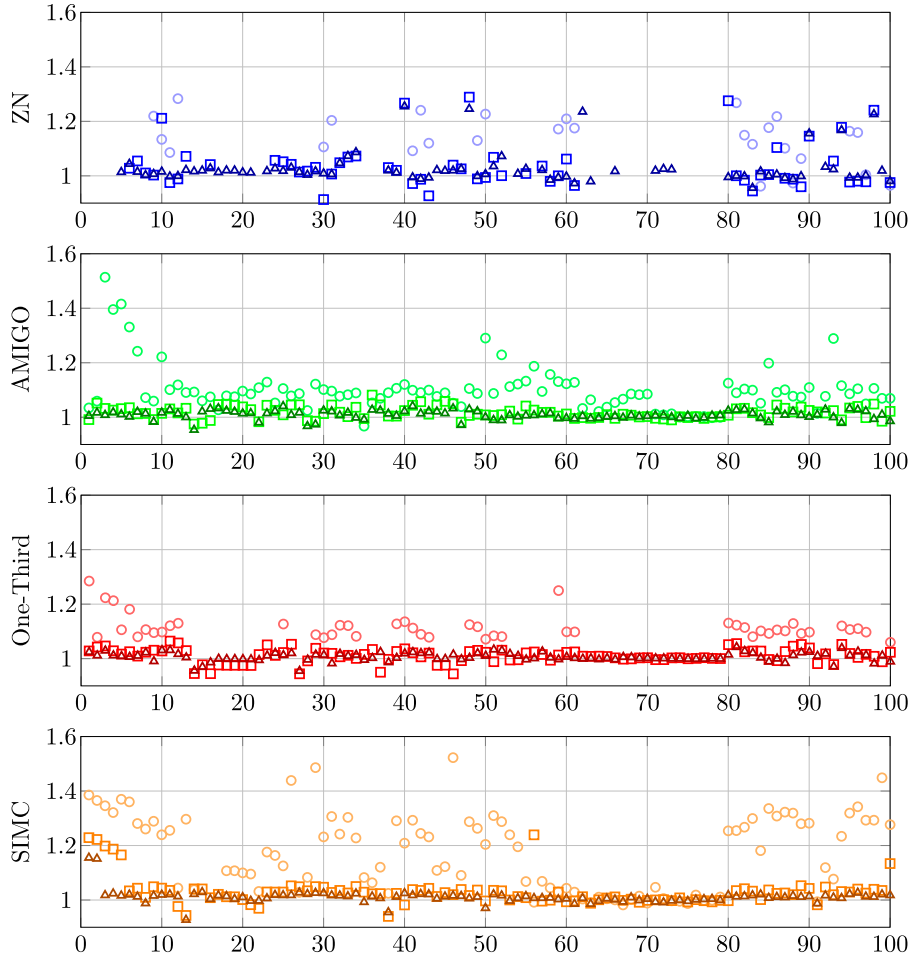


Figure 17. IAE^* for the batch of processes with different controllers (circles: $T_s = T_r/3$, squares: $T_s = T_r/10$, triangles: $T_s = T_r/20$).

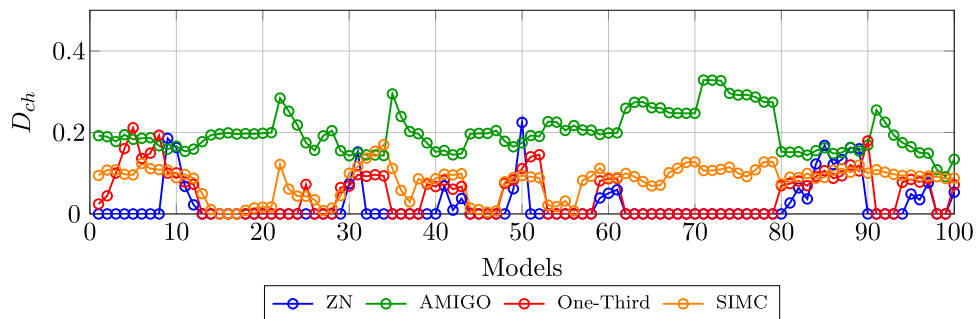


Figure 18. D_{ch} for the batch of processes with different controllers considering $T_s = T_r/3$.

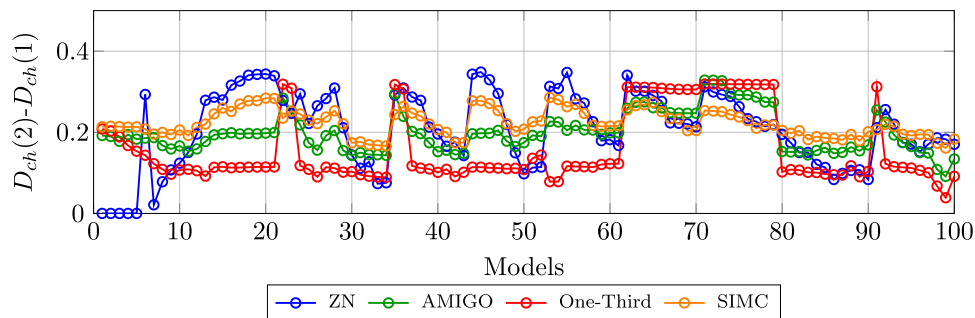


Figure 19. Difference between the robustness against oscillations of type $m = 2$ and of type $m = 1$.

parameters such as zeros and poles. Beyond the general considerations aforementioned, the admissible uncertainties in each parameter for a concrete model must be studied by an ad-hoc analysis.

5.3 Multi-levelled oscillations

The presented robustness study based on the proposed measure D_{ch} is substantiated on the assumption that by avoiding single-levelled oscillations (those with $m = 1$), multi-levelled oscillations ($m > 1$) will also be avoided. This fact was pointed out in Romero and Sanchis (2016) for the continuous case, but for the sampled case this study has not been addressed yet.

The definition of D_{ch} can be adapted to contemplate multi-levelled oscillations by considering only the traces of $-1/\mathcal{N}'$ of the level under study in Equation (13). Therefore, the robustness against, for instance, oscillations of two levels, can be determined by considering the cases where $m = 2$ in Equation (8) and obtaining their convex hulls, which will then be used to calculate the minimum distance to their respective critical point as explained in previous sections.

This variation of D_{ch} has been used to evaluate the robustness against two-levelled oscillations of processes in the batch presented in (14) with the controllers tuned with Ziegler–Nichols, AMIGO, One-Third and SIMC tuning rules. The difference between the robustness against limit cycle oscillations of two levels $D_{ch}(2)$ and single-levelled $D_{ch}(1)$ is presented in Figure 19. The measure $D_{ch}(1)$ is the same that presented in Figure 13.

From Figure 19, it can be observed an increase in the robustness in all cases. The unique cases where there is not an increase is on the first five processes tuned with Ziegler–Nichols method, which presented an oscillatory behaviour, and would also present it for $m = 2$. In the other cases, a generalised increase in the robustness margin is observed, proving that by avoiding single-levelled oscillations, multi-levelled oscillations are also avoided.

6. Conclusion

In this work, an approach to study the robustness of discrete event-based systems has been presented. The event generator under study is the Symmetric-Send-On-Delta quantifier and the controller has been implemented in a discrete fashion, which represents more accurately the current implementation of this kind of systems.

To perform the robustness analysis the Describing Function technique has been used, obtaining the Sampling Describing Function of the studied non-linearity. The characteristics of this Sampled DF have been studied, which ultimately presents characteristics similar to the continuous DF.

From the obtained Sampled DF and the stability condition several modifications have been made to facilitate the robustness analysis. First, the range to evaluate both the Sampled DF and the system under study have been bounded. Second, the scattered points resulting from the study have been grouped in a convex hull. Finally, a robustness measure has been established as the minimum of the distances to a convex hull. The validity of the approach has been tested through several examples.

Using this robustness measure, some well-known tuning rules have been evaluated, namely, Ziegler–Nichols, AMIGO, One-Third rule and SIMC. These tuning rules have been used to obtain the controllers for a wide batch of systems. To perform the discrete implementation, the sampling period has been chosen based on the rise time of the continuous system response. The obtained results reveal that Ziegler–Nichols tuning method struggles to offer controllers that avoid limit cycle oscillations. The other rules offer controllers with different levels of robustness, but they avoid consistently the apparition of limit cycle oscillations. In addition, it has been proved that the robustness of the controllers increases with the sampling frequency, behaviour that matches with the sampled control theory.

Despite the fact that some of the aforementioned tuning methods, e.g. AMIGO, avoid the limit cycles oscillation for most of the systems included in the studied batch, these methods does not take into account the condition to avoid limit cycles and it must be checked a posteriori. The robustness measure presented in this paper can be useful to define new tuning methods which consider the restriction on D_{ch} as a design requirement: $D_{ch} > D_{chr}$ where $D_{chr} > 0$ represents the required value of this robustness margin. Obviously, these new methods must also guarantee a good overall performance of the control systems.

Although the study presented in this paper considers the SSOD sampler, the sampled DF approach could be also applied for analysing the robustness to limit cycles when more general sampling strategies such as RQH are used, or even in the case of asymmetric multi-level relays.

Disclosure statement

No potential conflict of interest was reported by the author(s).

Funding

This work has been supported by research project 18I411-UJI-B2018-39 from Universitat Jaume I and by Conselleria d'Educació, Investigació, Cultura i Esport (CEICE) grant number ACIF/2018/244.

ORCID

Julio-Ariel Romero-Pérez  <http://orcid.org/0000-0003-3397-2239>

References

- Åström, K.J., & Hägglund, T. (2004). Revisiting the Ziegler–Nichols step response method for PID control. *Journal of Process Control*, 14(6), 635–650. <https://doi.org/10.1016/j.jprocont.2004.01.002>
- Astrom, K. J., & Wittenmark, B. (1997). *Computer-controlled systems: theory and design* (3rd ed.). Prentice Hall.
- Beschi, M., Dormido, S., Sánchez, J., & Visioli, A. (2012). Characterization of symmetric send-on-delta PI controllers. *Journal of Process Control*, 22(10), 1930–1945. <https://doi.org/10.1016/j.jprocont.2012.09.005>
- Beschi, M., Dormido, S., Sánchez, J., & Visioli, A. (2014a). Tuning of symmetric send-on-delta proportional-integral controllers. *IET Control Theory Applications*, 8(4), 248–259. <https://doi.org/10.1049/cth2.v8.4>
- Beschi, M., Dormido, S., Sanchez, J., Visioli, A., & Yebra, L. J. (2014b). Event-based pi plus feedforward control strategies for a distributed solar collector field. *IEEE Transactions on Control Systems Technology*, 22(4), 1615–1622. <https://doi.org/10.1109/TCST.2013.2279216>
- Beschi, M., Pawlowski, A., Guzmán, J. L., Berenguel, M., & Visioli, A. (2014). Symmetric send-on-delta pi control of a greenhouse system. *IFAC Proceedings Volumes*, 47(3), 4411–4416. <https://doi.org/10.3182/20140824-6-ZA-1003.0102819thIFACWorldCongress>
- Chacón, J., Sánchez, J., Visioli, A., Yebra, L., & Dormido, S. (2013). Characterization of limit cycles for self-regulating and integral processes with PI control and send-on-delta sampling. *Journal of Process Control*, 23(6), 826–838. <https://doi.org/10.1016/j.jprocont.2013.04.001>
- Dormido, S., Sánchez, J., & Kofman, E. (2008). Muestreo, control y comunicación basados en eventos. *Revista Iberoamericana de Automática e Informática Industrial RIAI*, 5(1), 5–26. [https://doi.org/10.1016/S1697-7912\(08\)70120-1](https://doi.org/10.1016/S1697-7912(08)70120-1)
- Gelb, A., & Van der Velde, W. E. (1968). *Multiple-input describing functions and non-linear system design*. McGraw-Hill.
- Hägglund, T. (2019). The one-third rule for PI controller tuning. *Computers & Chemical Engineering*, 127, 1125–30. <https://doi.org/10.1016/j.compchemeng.2019.03.027>
- Hägglund, T., & Åström, K. J. (2002). Revisiting the Ziegler–Nichols tuning rules for PI control. *Asian Journal of Control*, 4(4), 364–380. <https://doi.org/10.1111/asjc.2002.4.issue-4>
- Isermann, R. (1989). *Digital control systems: volume 1 fundamentals, deterministic control* (2nd ed.). Chapter choice of sample time for parameter-optimised control algorithms (pp. 151–154). Springer-Verlag Berlin Heidelberg GmbH.
- Kuo, B. C. (1960). The z-transform describing function for nonlinear sampled-data control systems. *Proceedings IRE*, 48(5), 941–942.
- Kuo, B. C. (1963). *Analysis and synthesis of sampled-data control systems*.
- McNamara, O. P., & Atherton, D. P. (1984). Limit cycles in non linear sampled data systems. *IFAC Proceedings Volumes*, 17(2), 507–512. [https://doi.org/10.1016/S1474-6670\(17\)61021-8](https://doi.org/10.1016/S1474-6670(17)61021-8)
- Miguel-Escrig, O., & Romero-Pérez, J.-A. (2020). Regular quantisation with hysteresis: a new sampling strategy for event-based pid control systems. *IET Control Theory & Applications*, 14(15), 2163–2175. <https://doi.org/10.1049/cth2.v14.15>
- Miguel-Escrig, O., & Romero-Pérez, J.-A. (2020). Regular quantisation with hysteresis: a new sampling strategy for event-based pid control systems. *IET Control Theory & Applications*, 14(15), 2163–2175. <https://doi.org/10.1049/cth2.v14.15>
- Miguel-Escrig, O., Romero-Pérez, J.-A., & Sanchis-Llopis, R. (2020). Tuning PID controllers with symmetric send-on-delta sampling strategy. *Journal of the Franklin Institute*, 357(2), 832–862. <https://doi.org/10.1016/j.franklin.2019.10.008>

- Ploennigs, J., Vasyutynskyy, V., & Kabitzsch, K. (2010). Comparative study of energy-efficient sampling approaches for wireless control networks. *IEEE Transactions on Industrial Informatics*, 6(3), 416–424. <https://doi.org/10.1109/TII.2010.2051812>
- Rodríguez-Miranda, E., Beschi, M., Guzmán, J. L., Berenguel, M., & Visioli, A. (2019). Application of a symmetric-send-on-delta event-based controller for a microalgal raceway reactor. In *2019 18th European control conference (ECC)* (pp. 3132–3137), IEEE.
- Rodríguez-Miranda, E., Beschi, M., Guzmán, J. L., Berenguel, M., & Visioli, A. (2019). Daytime/nighttime event-based pi control for the ph of a microalgae raceway reactor. *Processes*, 7(5), 247. <https://doi.org/10.3390/pr7050247>
- Romero, J. A., & Sanchis, R. (2016). A new method for tuning PI controllers with symmetric send-on-delta sampling strategy. *ISA Transactions*, 64, 1161–173. <https://doi.org/10.1016/j.isatra.2016.05.011>
- Romero, J. A., Sanchis, R., & Arrebola, E. (2015). Experimental study of event based pid controllers with different sampling strategies. Application to brushless dc motor networked control system. In *2015 XXV international conference on information, communication and automation technologies (ICAT)* (pp. 1–6), IEEE.
- Romero, J. A., Sanchis, R., & Penarrocha, I. (2014). A simple rule for tuning event-based PID controllers with symmetric send-on-delta sampling strategy. In *Proceedings of the 2014 IEEE emerging technology and factory automation (ETFA)* (pp. 1–8), IEEE.
- Romero Pérez, J. A., & Sanchis Llopis, R. (2017). Tuning and robustness analysis of event-based PID controllers under different event-generation strategies. *International Journal of Control*, 91(7), 1567–1587. <https://doi.org/10.1080/00207179.2017.1322716>
- Skogestad, S. (2003). Simple analytic rules for model reduction and PID controller tuning. *Journal of Process Control*, 13(4), 291–309. [https://doi.org/10.1016/S0959-1524\(02\)00062-8](https://doi.org/10.1016/S0959-1524(02)00062-8)
- Ziegler, J. G., & Nichols, N. B. (1942). Optimum settings for automatic controllers. *Transactions of the ASME*, 64(11), 759–768.

Appendix. Sampled DF calculation

The Sampled Describing Function which relates the input and output of the non-linear element in the system can be computed in the following way:

$$\mathcal{N}(\delta, A, T_s) = \frac{\text{Phasor representation of fundamental component of } \bar{e}^*}{\text{Phasor representation of } e}$$

First, the phasor representation of e can be easily obtained since for the DF calculations:

$$e(t) = A \sin(\omega_0 t) = A \cos\left(\omega_0 t + \frac{3\pi}{2}\right) = \Re \left\{ A e^{j(\omega_0 t + \frac{3\pi}{2})} \right\}.$$

For the phasor representation of the fundamental component of \bar{e}^* , an harmonic analysis using Fourier series has been done. Expressing $\bar{e}^*(t)$ as

$$\bar{e}^*(t) = \bar{e}(t) \cdot \delta_{PT}(t),$$

where the pulse train δ_{PT} is defined as

$$\delta_{PT}(t) = \sum_{k=-\infty}^{\infty} \delta_D(t - \tau - kT_s),$$

where δ_D is the Dirac delta function, T_s is the sampling period and τ the time lag between the initial zero-crossing of $e(t)$ and the first sample (which is bounded between 0 and T_s).

To obtain the fundamental component of $\bar{e}^*(t)$, first we obtain the Fourier series representing $\bar{e}(t)$:

$$\hat{\bar{e}}(t) = -\frac{\delta}{j\pi} \sum_{n=-\infty}^{\infty} \frac{1}{n} \left\{ \sum_{i=1}^m i [e^{-jn\omega_0 t_{i+1}} - e^{-jn\omega_0 t_i}] \right. \\ \left. + \sum_{i=m+1}^{2m-1} (2m-i) [e^{-jn\omega_0 t_{i+1}} - e^{-jn\omega_0 t_i}] \right\} e^{jn\omega_0 t},$$

where t_n are the times where level switches are produced. And second, we obtain the Fourier series representation of δ_{PT} is:

$$\hat{\delta}_{PT}(t) = \frac{1}{T_s} \sum_{k=-\infty}^{\infty} e^{jk\omega_s(t-\tau)}.$$

Multiplying both:

$$\begin{aligned} \hat{e}^*(t) = & -\frac{\delta}{j\pi T_s} \sum_{k=-\infty}^{\infty} \sum_{n=-\infty}^{\infty} \frac{1}{n} \left\{ \sum_{i=1}^m i \left[e^{-jn\omega_o t_{i+1}} - e^{-jn\omega_o t_i} \right] \right. \\ & \left. + \sum_{i=m+1}^{2m-1} (2m-i) \left[e^{-jn\omega_o t_{i+1}} - e^{-jn\omega_o t_i} \right] \right\} e^{jn\omega_o t} e^{jk\omega_s(t-\tau)}. \end{aligned}$$

To obtain the fundamental harmonic from this expression we have to pay attention to the exponents that imply the variable t , which can be grouped in a single expression:

$$j(n\omega_o + k\omega_s)t - jk\omega_s\tau.$$

Then, the part that multiplies t has to be the fundamental frequency, i.e. either $+\omega_o$ or $-\omega_o$. Taking r as the ratio between the oscillation and sampling period ($r = T_o/T_s$) we can obtain the relation between the harmonics of the sampling (k) and of the signal $\tilde{e}(t)$ (n) to obtain the fundamental frequency of $\tilde{e}^*(t)$:

$$\begin{aligned} n\omega_o + k\omega_s &= \omega_o & n\omega_o + k\omega_s &= -\omega_o \\ n + k \frac{\omega_s}{\omega_o} &= 1 & n + k \frac{\omega_s}{\omega_o} &= -1 \\ n &= 1 - kr & n &= -1 - kr \end{aligned}$$

Thus the relation of harmonics to consider are both $n = 1 - kr$ and $n = -1 - kr$. The expression of the fundamental harmonic of $\tilde{e}^*(t)$ is

$$\begin{aligned} \hat{e}^*(t) = & -\frac{\delta}{j\pi T_s} \sum_{k=-\infty}^{\infty} \left\{ \frac{1}{1-kr} \left\{ \sum_{i=1}^m i \left[e^{-j(1-kr)\omega_o t_{i+1}} - e^{-j(1-kr)\omega_o t_i} \right] \right. \right. \\ & \left. \left. + \sum_{i=m+1}^{2m-1} (2m-i) \left[e^{-j(1-kr)\omega_o t_{i+1}} - e^{-j(1-kr)\omega_o t_i} \right] \right\} e^{j\omega_o t} \right. \\ & \left. + \frac{1}{-1-kr} \left\{ \sum_{i=1}^m i \left[e^{-j(-1-kr)\omega_o t_{i+1}} - e^{-j(-1-kr)\omega_o t_i} \right] \right. \right. \end{aligned}$$

$$\begin{aligned} & \left. + \sum_{i=m+1}^{2m-1} (2m-i) \left[e^{-j(-1-kr)\omega_o t_{i+1}} - e^{-j(-1-kr)\omega_o t_i} \right] \right\} e^{-j\omega_o t} \Bigg\} \\ & \times e^{-jk\omega_s\tau}. \end{aligned}$$

Taking into account that:

$$e^{-j(1-kr)\omega_o t_i} = (e^{j\omega_o t_i})^{rk-1} = (\cos(\omega_o t_i) + j \sin(\omega_o t_i))^{rk-1}$$

and

$$\begin{aligned} \sin(\omega_o t_i) &= \begin{cases} \frac{i\delta}{A} & \text{if } i = 1, 2, \dots, m \\ (2m-i) \frac{\delta}{A} & \text{if } i = m+1, m+2, \dots, 2m \end{cases} \\ \cos(\omega_o t_i) &= \begin{cases} +\sqrt{1 - \left(\frac{i\delta}{A}\right)^2} & \text{if } i = 1, 2, \dots, m \\ -\sqrt{1 - \left((2m-i) \frac{\delta}{A}\right)^2} & \text{if } i = m+1, m+2, \dots, 2m \end{cases} \end{aligned}$$

the expression of $\hat{e}^*(t)$ can be simplified and its phasor representation obtained after some straightforward algebra calculus. Then the ratio between the phasor of $\hat{e}^*(t)$ and the phasor of $e(t)$ resulting in the Sampled DF:

$$\begin{aligned} \mathcal{N}(\delta/A, r, \tau, T_s) &= \frac{2\delta}{\pi T_s A} \sum_{k=-\infty}^{\infty} \frac{e^{-jk2\pi\tau/T_s}}{rk-1} \\ & \times \left[\sum_{i=1}^{m-1} \left\{ \left(-\sqrt{1 - \left(\frac{i\delta}{A}\right)^2} + j \frac{i\delta}{A} \right)^{rk-1} \right. \right. \\ & \left. \left. - \left(\sqrt{1 - \left(\frac{i\delta}{A}\right)^2} + j \frac{i\delta}{A} \right)^{rk-1} \right\} \right. \\ & \left. - \left(\sqrt{1 - \left(\frac{m\delta}{A}\right)^2} + j \frac{m\delta}{A} \right)^{rk-1} + (-1)^{rk-1} \right]. \end{aligned}$$